Austenite Grain Growth in a 2.25Cr-1Mo Vanadium-Free Steel Accounting for Zener Pinning and Solute Drag: Experimental Study and Modeling

S. DÉPINOY, B. MARINI, C. TOFFOLON-MASCLET, F. ROCH, and A.-F. GOURGUES-LORENZON

Austenite grain size has been experimentally determined for various austenitization temperatures and times in a 2.25Cr-1Mo vanadium-free steel. Three grain growth regimes were highlighted: limited growth occurs at lower temperatures [1193 K (920 °C) and 1243 K (970 °C)]; parabolic growth prevails at higher temperatures [1343 K (1070 °C) and 1393 K (1120 °C)]. At the intermediate temperature of 1293 K (1020 °C), slowed down growth was observed. Classical grain growth equations were applied to the experimental results, accounting for Zener pinning and solute drag as possible causes for temperature-dependent limited growth. It was shown that Zener pinning due to AlN particles could not be responsible for limited growth, although it has some effect at lower temperatures. Instead, limited and slow growths are very likely to be the result of segregation of molybdenum atoms at austenite grain boundaries. The temperature-dependence of this phenomenon may be linked to the co-segregation of molybdenum and carbon atoms.

I. INTRODUCTION

Light water reactors are representing 80 pct of the world nuclear power plants. On an international level, the renewal of second-generation light water reactors is to be provided by light water reactors until at least the middle of the century. Thus, safety and technological improvement of these reactors represent key issues in electrical power generation. In this framework, the 2.25Cr-1Mo steel family, already widely used in the petrochemical industry, is being considered as a potential candidate pressure vessel material for future light water reactors. The two main reasons are its good mechanical properties in the quenched and tempered conditions[1] and its very good resistance to radiation-induced embrittlement compared to usual pressure vessel steels due to its low Ni content and low residuals.[2]

Quenched and tempered 2.25Cr-1Mo steels are fully bainitic, which leads to optimum tensile and toughness properties, as well as creep resistance, compared to a proeutectoid ferritic bearing materials.[3,4] However, during water quench of thick-walled components such as pressure vessels, a gradient in cooling rate takes place across the wall thickness and may lead to the formation of ferrite. While the occurrence of 2 pct proeutectoid ferrite does not change the mechanical properties,[5] it is generally advised to minimize the proeutectoid ferrite fraction.[6] A convenient way to control transformations upon quenching is by increasing the austenite grain size prior to the quench, as coarser austenite grains delay the ferritic transformation toward slower cooling rates.[7,8] However, and while the austenite grain size has no direct impact on the subsequent carbide precipitation during tempering[9,10] and on the tensile properties of 2.25Cr-1Mo steels,[8–11] too coarse grains can decrease the toughness,[8,11] increase the susceptibility to temper embrittlement,[12] increase the bainitic packet size[9,11] and may lead to formation of martensite[7,9] after quenching. Additionally, the austenite grain size has to be constant across the wall thickness of the considered component in order to ensure homogeneous microstructure and mechanical properties after quenching. Thus, austenite grain growth must be understood in order to control the austenite grain size through austenitization time and temperature.

Very few data have been reported about the effect of austenitization conditions on austenite grain size for 2.25Cr-1Mo steels. Most results come from studies where only few different values of austenite grain size were used for subsequent investigations of other properties, such as resistance to temper embrittlement, toughness properties, or effect of additional alloying elements, for instance.[8,12–17] Moreover, only two attempts at modeling austenite grain growth in 2.25Cr-1Mo can be found in the literature. The first one, by Miranda and Fortes,[18] uses an empirical

S. DÉPINOY, is with the DEN-Service de Recherches Métallurgiques Appliquées, CEA, Université Paris-Saclay, 91191 Gif sur Yvette, France, and also with the MINES ParisTech, PSL Research University-Centre des Matériaux, UMR CNRS 7633, 9 BP 87, 91003 Evry cedex, France. B. MARINI and C. TOFFOLON-MASCLET are with the DEN-Service de Recherches Métallurgiques Appliquées, CEA, Université Paris-Saclay, Contact e-mail: sdepinoy@gmail.com F. ROCH is with AREVA, 1 place Jean Millier 92084 Paris La Défense Cedex. A.-F. GOURGUES-LORENZON is with MINES ParisTech, PSL Research University-Centre des Matériaux, UMR CNRS 7633, BP 87, 91003 Evry Cedex, France.

approach in order to model the austenite grain size in heat affected zones during welding. The other one, by Sista et al.,[19] reproduces Miranda and Fortes's results using Monte-Carlo methods. However, these results are not directly applicable to the present case, as they involve very fast heating rates and very short austenitization times, while heat treatments of thick-walled components involve low heating rates and long austenitization times (e.g., at least a fraction of an hour).

This work is dedicated to the experimental characterization of austenite grain growth of a vanadium-free 2.25Cr-1Mo with time at various austenitization temperatures. Mathematical models are then applied in order to determine the physical mechanisms controlling grain growth and for predicting the austenite grain size for a given austenitization conditions.

II. MATERIAL AND PROCEDURES

The material, which chemical composition is given in Table I, comes from the quarter-thickness of a 280-mm-thick forged ring, fabricated from a hollow ingot cast by bottom pouring. The as-received microstructure is tempered bainite, with a prior austenite grain size ranging between 30 and 50 μm.

Prior austenite grains were measured after further austenitization at temperatures ranging from 1193 K (920 °C) to 1393 K (1120 °C) and for durations up to 2 hours. The heating rate was set to 1 K/s, and the corresponding Ac_3 temperature was determined to be 1153 K (880 °C). Heat treatments were performed in air on a DT1000 dilatometer from (AET Technologies) using $12 \times 2 \times 2$ mm^3 samples.

As the austenitic phase in the studied steel is not stable at ambient temperature, no direct observation of austenite grains was possible. To address this issue, an interrupted quenching procedure was applied: after austenitization, the sample was quenched at 50 K/s in the dilatometer down to and held at an intermediate temperature, before a final quench at 50 K/s down to room temperature. The objective was to precipitate small ferrite grains at austenite grain boundaries. The selected isothermal holding conditions (898 K (625 °C), 48 hours) were chosen using a TTT diagram established for the 1193 K (920 °C)—30 minutes austenitization condition (Figure 1). They lead to partial decomposition of austenite into ferrite, with a greater contribution from nucleation over that of growth. The final quench transformed the remaining austenite into martensite. The microstructure was then revealed by dipping cut and polished samples for a few seconds into an aqueous solution of sodium disulfide. This tinting etchant colors ferrite in dark brown and martensite in light brown.

It should be kept in mind that any increase in austenite grain size obviously affects the precipitation of

Table I. Chemical Composition of the Studied Material (in Wt Pct)

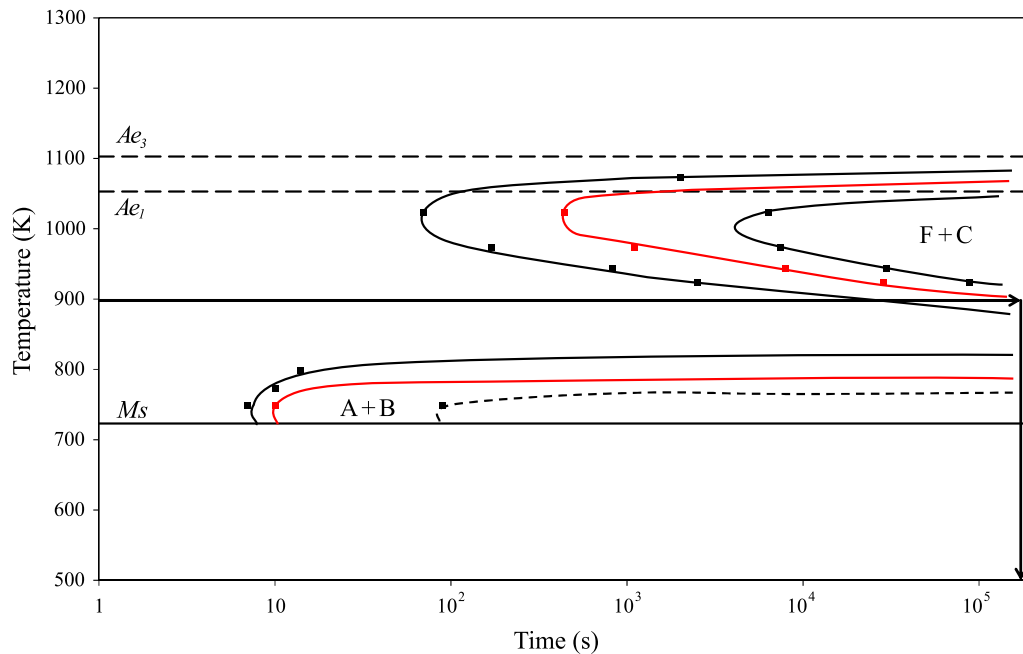| C	Cr	Mo	Mn	Ni	Si	Al	N	P	S	V
0.15	2.47	1.11	0.51	0.17	0.24	0.008	0.007	0.006	0.003	<0.01

Fig. 1—TTT diagram of the studied steel after an austenitization at 1193 K (920 °C) for 30 min. A: austenite, B: bainite, F: ferrite, C: carbides. Intermediate curve in each domain represents 50 pct of transformed austenite, and the arrows represent the isothermal holding at 898 K (650 °C) used in this study.

ferrite by shifting the ferritic transformation domain toward higher temperatures and times. For larger austenite grains, it means that less ferrite nucleates thus austenite grain boundaries are not so well defined. For smaller austenite grains, there is a high risk that ferritic grains grow at the expense of austenite grains, partly masking their original morphology and size, so that no measurements can be done. All austenitization conditions were first followed by the isothermal holding. When this method was suspected to be inefficient, *i.e.*, when small austenite grain sizes were found (typically, for austenitization times up to 5 minutes), additional samples were quenched at 50 K/s to room temperature right after the austenitization step, and then lightly etched with Villela etchant.

A least six optical micrographs (2080 × 1544 pixels) were taken for each austenitization condition. The magnification was selected according to the grain size: for coarse grains as the ones obtained after austenitization at 1393 K (1120 °C), images were taken using a 100 times magnification. Otherwise, a 200 times magnification was used. Austenite grain size was then measured using the Visilog software. Each grain was measured individually and then the average grain size was calculated. Between 60 and 800 grains were measured per condition. The maximum uncertainty associated with measurements was estimated around 5 μm, due to the size of ferrite nodules that formed during interrupted quenching.
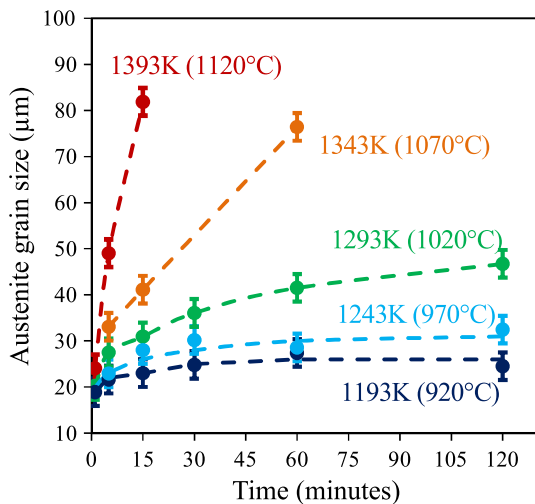

Fig. 2—Evolution of austenite grain size with austenitization time and temperature.

III. EXPERIMENTAL RESULTS

The evolution of average prior austenitic grain size (PAGS) with austenitization temperature and time is presented in Figure 2 and Table II. The results are in the same order of magnitude compared to the few data about austenite grain size reported in the literature for similar vanadium-free 2.25Cr-1Mo steels, which are gathered in Table III.

The value of austenite grain size at the beginning of the isothermal austenitization step, namely about 20 μm, is likely related to the slow heating rate that was used to be representative of the actual thermal cycle experienced in thick-walled components. As a result, the so-called initial austenite grain size (*i.e.*, at the beginning of soaking) slightly increases from 19 to 26 μm with increasing soaking temperature.

At low temperatures, *i.e.*, $T \leq 1293$ K (1020 °C), grain growth kinetics decreases with decreasing temperature. At 1193 K (920 °C), almost no growth occurs. At high temperatures, *i.e.*, $T \geq 1343$ K (1070 °C), the growth law is parabolic. However, the maximal studied austenitization time at these temperatures is 1 hour, and limited growth is still susceptible to appear for longer austenitization durations. The above results suggest the existence of a temperature-dependent phenomenon which is responsible for limited growth and becomes less efficient with increasing temperature.

Examples of obtained microstructures and corresponding grain size distributions are shown in Figure 3. Grain size histograms can be correctly described by a lognormal density functions for all studied austenitization conditions, and thus, no abnormal growth occurs and the austenite grain size distribution can be characterized in a representative way using the average PAGS. Moreover, it is remarkable that the coefficient of variation (ratio of the standard deviation to the mean value) of these distribution is only slightly time dependent for all tested conditions (Figure 4). Due to experimental uncertainties

Table III. Austenite Grain Size Corresponding to Different Austenitization Heat Treatments as Reported in the Literature

Sources	Heat Treatment	PAGS (μm)
8	1248 K (975 °C): 120 min	20
	1323 K (1050 °C): 120 min	90
	1473 K (1200 °C): 120 min	310
12	1223 K (950 °C): 120 min	25
	1373 K (1100 °C): 120 min	120
	1523 K (1250 °C): 120 min	155

Table II. Experimentally Determined Austenite Grain Size for the Studied Austenitization Heat Treatments

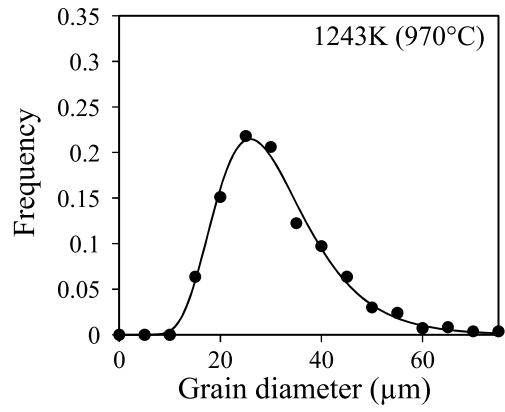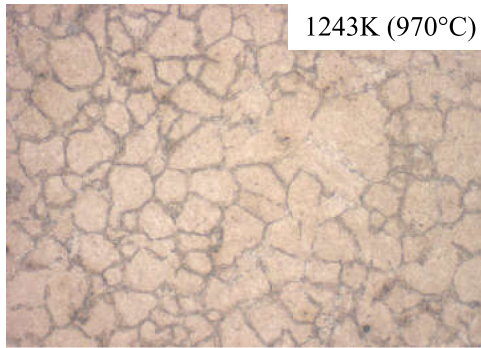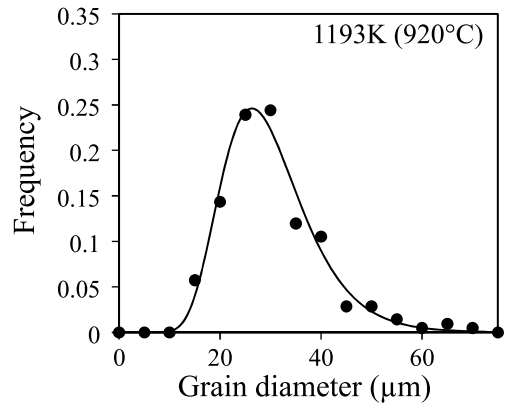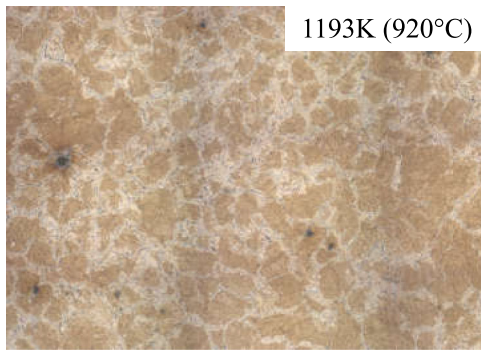| Temperature	1 min	5 min	15 min	30 min	60 min	120 min
1193 K (920 °C)	19 μm	22 μm	23 μm	25 μm	27 μm	25 μm
1243 K (970 °C)		23 μm	28 μm	30 μm	29 μm	32 μm
1293 K (1020 °C)	20 μm	28 μm	31 μm	36 μm	42 μm	47 μm
1343 K (1070 °C)		33 μm	41 μm		76 μm	
1393 K (1120 °C)	24 μm	49 μm	82 μm			
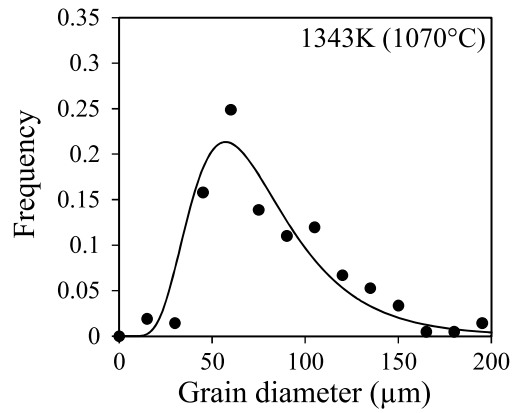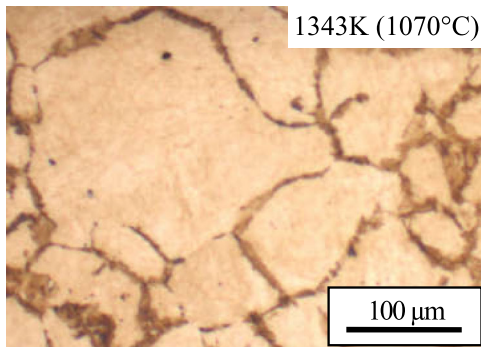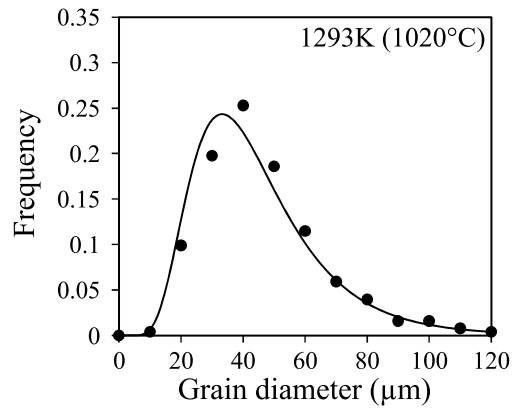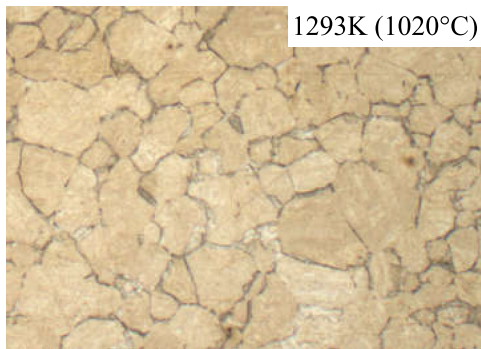
Fig. 3—Microstructure and grain size distribution after austenitization at various temperatures for 60 min followed by isothermal holding at 898 K (625 °C) for 48 h. Ferrite in dark brown, except for austenitization at 1193 K (920 °C).

and at least for the three lowest temperatures, it can be considered as constant and equal to 0.36. Then the prediction of the mean value could be sufficient to give an evaluation of the whole distribution. As a consequence, only mean values are considered in the following.

IV. MODELING AUSTENITE GRAIN GROWTH

A. *Equations and Selection of Parameters*

For normal grain growth in polycrystalline materials, a very simple model may be used to describe the growth of a single grain, assuming that its diameter D is representative of all grains in the material.

Under this assumption, it is considered that the boundary of a grain of radius $D/2$ moves with a velocity v due to the net pressure P acting on it. It is generally assumed that the velocity is directly proportional to the pressure with the constant of proportionality being the mobility M of the boundary (Eq. [1]). In this study, the net pressure consists of the difference between the driving pressure, P_d, and the retarding pressures due to Zener pinning, P_z, and to solute drag, P_{drag} (Eq. [2]):

$$\frac{1}{2}\frac{dD}{dt} = v = MP, \qquad [1]$$

$$\frac{1}{2}\frac{dD}{dt} = v = M(P_d - P_z - P_{drag}). \qquad [2]$$

1. *Grain boundary mobility*

The mobility is strongly temperature dependent and follows an Arrhenius-type relationship, as shown in Eq. [3]:

$$M = M_0 \exp\left(-\frac{Q}{RT}\right). \qquad [3]$$

It is generally assumed that the activation energy for boundary migration is often close to that of grain boundary self-diffusion, which is about half that of lattice self-diffusion.[20] Thus, in austenite, the activation energy for grain growth is expected to be in the range of 145 to 170 kJ mol^{-1}. In alloyed steels, empirical activation energies experimentally determined are usually higher than the above values, typically, between 250 and 500 kJ mol^{-1}.[21] This deviation is believed to be due to the diffusion of impurity atoms, or to the fact that the diffusion of atoms is *across* a *moving* grain boundary, and not *along* a *static* one.

2. *Driving pressure*

For the considered spherical grain of diameter D, the driving pressure resulting from the boundary curvature can be written as follows:

$$P_d = 4\frac{\gamma_g}{D}, \qquad [4]$$

where γ_g is the grain boundary interfacial energy. The value of γ_g was set to 0.5 J m^{-2}[20] since it was successfully used in various calculations for grain growth in low-alloy steels.[22–24]

3. *Pinning pressure*

The pinning effect, theorized by Zener and published by Smith,[25] assumes that second phase particles exert a pressure on the grain boundary and thus counteract the driving pressure for grain growth. For particles of equivalent radius r_p and particle/matrix interfacial energy γ_p per unit area, the pinning pressure is as follows:

$$P_z = k_r\frac{\gamma_p f}{r_p}, \qquad [5]$$

where k_r is a dimensionless pinning parameter that depends on the particle shape and coherency with the matrix, but also on the physical interaction mechanisms between the particle and the matrix, as well as on the
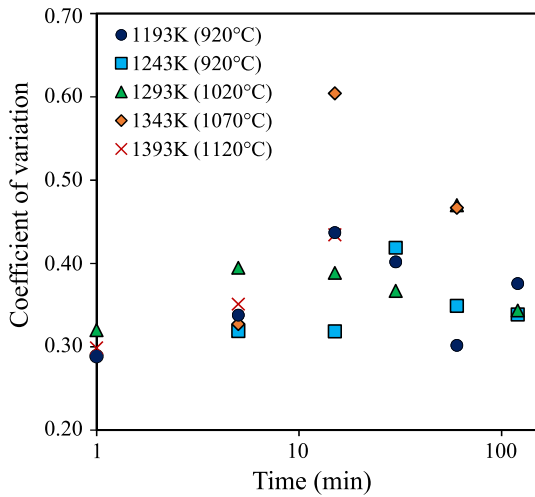

Fig. 4—Evolution of coefficient of variation with austenitization conditions.
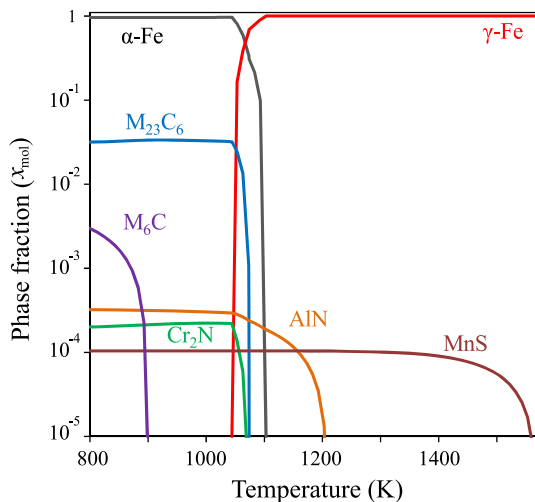

Fig. 5—Phase stability diagram predicted using MatCalc software for the studied steel composition.
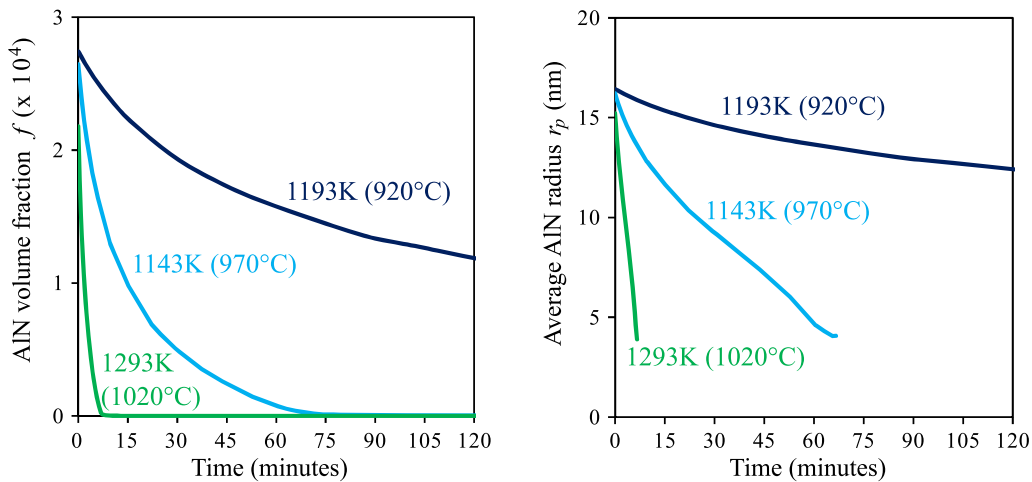
Fig. 6—Evolution with time and temperature of the volume fraction and average particle radius of AlN particles as predicted by thermokinetic calculations.
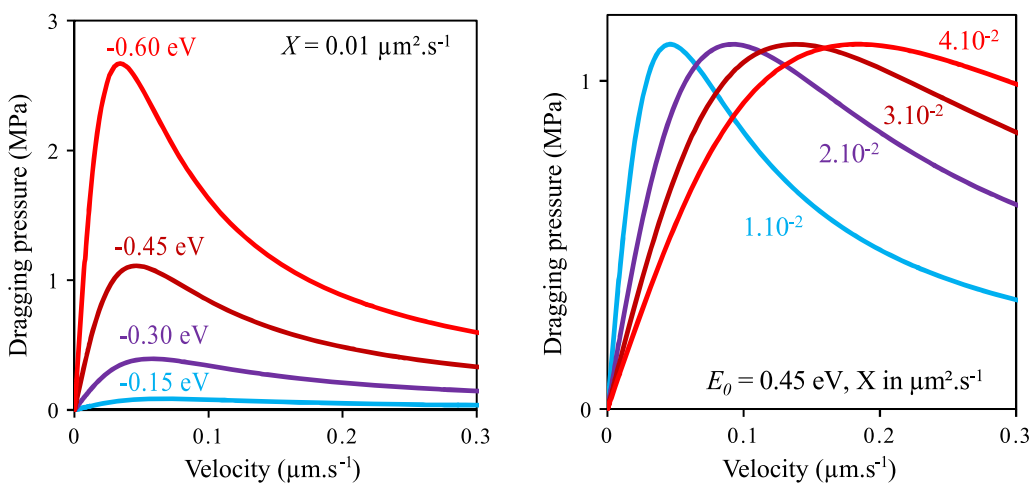

Fig. 7—Effect of the binding energy $-E_0$ (in eV) and of the diffusion coefficient X on the dragging pressure as a function of the grain boundary velocity.

interaction geometry between the particle and the matrix in the case of non-spherical particles. Note that in the original equation derived from Zener's work on incoherent spherical particles, $k_r = 3/2$. A large variety of values for this parameter has been extensively summarized by Manohar et al.[26]

Equation [5] has since been widely used to model Zener pinning in microalloyed steels,[21–24,27–29] typically due to nitrides such as AlN or TiN or carbonitrides such as Nb(N, C) or V(N, C). Experimentally, the impacts of AlN and Nb(N,C) particles on austenite grain growth in a 2.25Cr-1Mo steel were, respectively, outlined by Swift[13] and Nieuwland et al.[16] Some authors also suggested that residual alloy carbides[7] or impurity particles, such as MnS,[17] could act as pinning particles. The studied material is vanadium- and niobium-free. To determine the nature of particles that could hinder austenite grain growth for the considered steel chemistry, thermodynamic calculations performed using MatCalc v.6.00, using the mc_fe_v2.029 database, are shown in Figure 5. Alloy carbides are

thermodynamically unstable at temperatures higher than 1023 K (750 °C) and are thus unlikely to act as pinning particles even at temperatures as low as 1193 K (920 °C). The same conclusion can be drawn for MnS particles due to their very low phase fraction. Therefore, potential pinning effect in the studied steel could only be induced by AlN precipitates. It must, however, be pointed out that these precipitates are only thermodynamically stable up to 1203 K (930 °C), and thus are not expected to play a significant role at higher temperatures.

The volume fraction f, the average radius r_p, and the particle energy γ_p of AlN precipitates were estimated as a function of austenitization time and temperature using the precipitation kinetics module of MatCalc. More detailed information on the underlying model can be found in Reference 30. The evolution of the f and r_p at 1193 K (920 °C), 1243 K (970 °C), and 1293 K (1020 °C) are reported in Figure 6. As expected from the thermodynamic calculations, AlN quickly dissolve at temperatures higher than 1203 K (930 °C); they are

Table IV. Summary of Available Literature Data on the Binding Energy of Molybdenum with a Grain Boundary in Ferrous Alloys

Sources	Binding Energy E_0 (eV)	Note
41	0.01 0.2	Extracted from literature data on Mo-P interaction. The first value corresponds to the binding energy of molybdenum alone, while the second one is an effective energy accounting for the carbon-molybdenum interaction
40	0.15 ± 0.03 (0.18 ± 0.03)	Extracted from experimental measurements on Fe-C-Mo steels, using a binding energy for carbon of 0.2 eV (0.1 eV). Austenitic matrix
42	0.17	Used in the modeling of the solute drag-like effect in a Fe-C-Mo system at austenite/ferrite boundaries
36	0.29 ± 0.02	Effective binding energy extracted from experimental measurements in Fe-C-Mo steel at 1073 K (800 °C). Ferritic matrix.
43	0.31	Predicted for 11 pct Cr-0.5 Mo steel. Ferritic matrix
44	0.43	Predicted using strain-field arguments. Austenitic matrix
45	0.5	Effective binding energy accounting for the interaction with carbon at 873 K (600 °C). Austenite/ferrite boundary
46	From 0.45 to 1.3	Ab-initio calculations at different locations on a grain boundary. Austenitic matrix.

fully dissolved after 75 and 7 minutes at 1243 K (970 °C) and 1293 K (1020 °C), respectively. At even higher temperatures, namely 1343 K (1070 °C) and 1393 K (1120 °C), AlN particles are dissolving during the first seconds of austenitization, and are thus not represented in Figure 6. The interfacial energy γ_p is not time dependent; however, it slightly changes with temperature, from 0.47 to 0.49 J m^{-2} at 1193 K (920 °C) and 1293 K (1020 °C), respectively.

AlN particles are assumed to be cuboid shaped[31]; therefore, the parameter k_r varies between 0.5 and 4.5 with an average value of 3 depending on the orientation of the particles with respect to the grain boundary and their coherency with both the shrinking and the growing grains, based on geometrical considerations made on Reference 32. A parametric study on the influence of the parameter k_r was made and led to qualitatively similar results; thus, the average value of 3 for this parameter was chosen for further calculations.

4. Solute drag

Solute element atoms can segregate from the bulk lattice to the grain boundary where they can be better accommodated. In the case of a moving boundary, segregated solute atoms may be dragged along and the grain boundary migration rate can be limited by the diffusivity of these dragged solute atoms. The pressure induced by the solute drag depends on the boundary velocity. For low values of velocity, the dragging pressure increases proportionally with the velocity, due to the increasing concentration of solute atoms at the boundary, and reaches a maximal pressure for a critical velocity. For higher velocities, solute atoms find it more and more difficult to keep pace with the migrating boundary, resulting in their desorption from the grain boundary. The dragging pressure thus starts to decrease and then finally vanishes when no more solute atoms are segregating at the moving grain boundary. Cahn[33] approximated the following expression of the solute drag pressure, P_{drag}:

$$P_{drag} = \frac{C_0 \alpha v}{1 + \beta^2 v^2}, \quad [6]$$

where C_0 is the bulk concentration of solute atoms, α and β are parameters which depend on the number of atoms per unit volume, given as $N_v = 4/a^3$, where a is the lattice parameter assuming a fcc crystal structure, on the binding energy profile between the solute atom and the boundary $E(z)$, where z is the distance to the boundary, on the solute element diffusion coefficient profile $X(z)$, on the Boltzmann constant k and on temperature. Assuming (i) that X is constant across a grain boundary of thickness δ and (ii) a triangular profile for $E(z)$ with a minimal value $-E_0$ for $z = 0$ and a zero value for $z \leq -\delta/2$ and for $z \geq +\delta/2$, α and β are given by the following equations*:

---

*In the original article, Cahn wrote Eq. [7] as $\alpha = \frac{N_v(kT)^2}{E_0 X}\left(\sinh\left(\frac{E_0}{kT}\right) - \frac{E_0}{kT}\right)$. However, such equation is not dimensionally homogeneous with Eq. [6]. Therefore, this equation has been multiplied by the grain boundary thickness δ in order to obtain the right dimension for α. A similar correction has already been made by Fu et al.[49]

$$\alpha = \frac{N_v(kT)^2 \delta}{E_0 X}\left(\sinh\left(\frac{E_0}{kT}\right) - \frac{E_0}{kT}\right), \quad [7]$$

$$\beta^2 = \frac{\alpha k T \delta}{2 N_v E_0^2 X}. \quad [8]$$

In order to represent the effects of E_0 and X on the dragging pressure for the considered profile, let us assume that $C_0 = 0.1$ at. pct, $a = 0.36$ nm, $\delta = 0.5$ nm, and $T = 1273$ K (1000 °C). Figure 7 shows the dragging pressure as a function of the grain boundary velocity when varying the binding energy E_0 and the
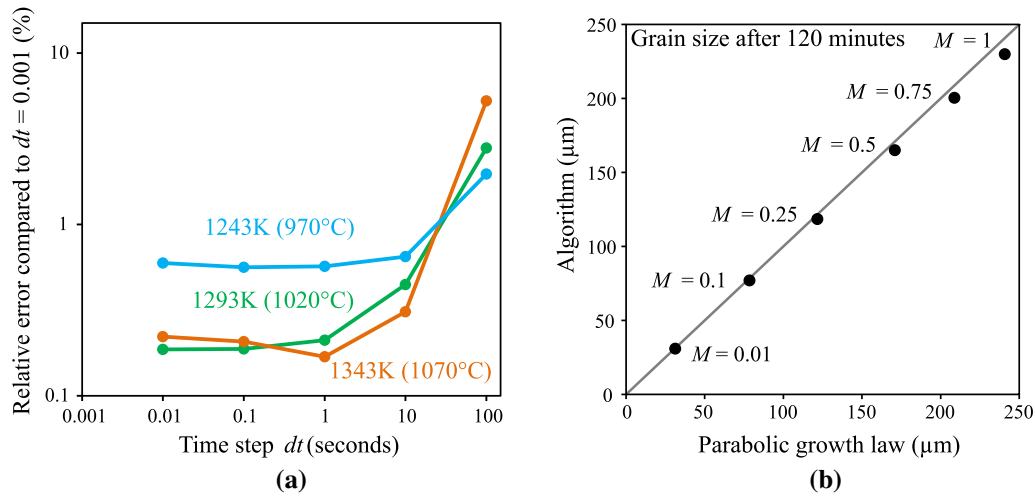
Fig. 8—(*a*) Time convergence analysis for the algorithm at 1243 K (970 °C), 1293 K (1020 °C), and 1343 K (1070 °C) using the parameters given in Table V. Grain size were calculated for $t = 1000$ s (16.6 min) for time step ranging 0.001 s to 100 s. This duration was chosen as it corresponds to the time the limited growth begins (Fig. 2). (*b*) Comparison between austenite grain size for $t = 120$ min as predicted by the parabolic growth law and the algorithm for $E_0 = -0.01$ eV, $T = 1173$ K (900 °C), $P_z = 10^{-3}$ MPa, and d$t = 0.1$ s. Mobility values are expressed in 10^{-12} m^4 J^{-1} s^{-1}.

Table V. Mobility M and Binding Energy E_0 Adjusted on Experimental Data for Each Temperature

Temperature	1193 K (920 °C)	1243 K (970 °C)	1293 K (1020 °C)	1343 K (1070 °C)	1393 K (1120 °C)
M (10^{-12} m^4 J^{-1}.s^{-1})	0.05	0.12	0.19	0.4	0.75
E_0 (eV)	−0.45	−0.43	−0.42	−0.30	−0.10

diffusion coefficient X. Increasing the binding energy leads to an increase in the maximal dragging pressure, while increasing the solute diffusivity shifts the critical velocity toward higher values. In other words, solute atoms induce more dragging when they are well accommodated in the boundary, and the boundary needs to move faster to break free from solute atoms when their diffusivity in the grain lattice close to this grain boundary is higher.

Molybdenum is commonly seen as an element that can induce solute drag[34] due to its large atomic mismatch with the austenite matrix, and is known for segregating at austenite grain boundaries.[35–37] In 2.25Cr-1Mo steels, an average concentration of 2 at. pct Mo was measured at the prior austenite grain boundaries after austenitization at 1423 K (1150 °C) for 2 hours followed by water quench.[38] While the authors supposed that a large amount of this segregation occurred upon quenching, at least some of this molybdenum may have segregated during austenitization.

The diffusion coefficient for molybdenum in austenite in cm^2 second^{-1} is given as[39]

$$X_{\text{Mo}/\gamma} = 0.482 \exp\left(-\frac{269,833}{RT}\right), \quad [9]$$

where T is in Kelvin and R is the gas constant. Reported values for the binding energy are summarized in Table IV and range between 0.01 and 1 eV. However, Enomoto *et al.*[40] showed that segregation of

molybdenum atoms at austenite grain boundaries was enhanced by the presence of carbon. Thus, in the following study the binding energy of molybdenum should account for this interaction, and therefore the effective binding energy is likely in the range of 0.15 up to 0.5 eV.

The other model parameters are the atomic solute concentration of Mo in the bulk, $C_0 = 0.006$, the lattice parameter of austenite, $a = 0.36$ nm, and the effective boundary thickness which is assumed to be $\delta = 0.5$ nm.

B. Setting up the Model

From the above equations, the boundary velocity v can be written as follows:

$$v = M\left(k_d\gamma_g \frac{1}{D} - k_r\gamma_p \frac{f}{r_p} - \frac{C_0\alpha v}{1 + (\beta v)^2}\right). \quad [10]$$

Among the total pressure contributions, the Zener pressure P_z is the only one whose value is not dependent on the grain size or on its time derivative, although it evolves with time due to an evolution of pinning particles themselves. Assuming that for each time step i, the grain diameter $D_i = D_{i-1} + 2v_i dt$ and that $P_z = P_z(i)$, then Eq. [10] can be written as a fourth degree polynomial of the grain boundary velocity v_i for each time step i, such as
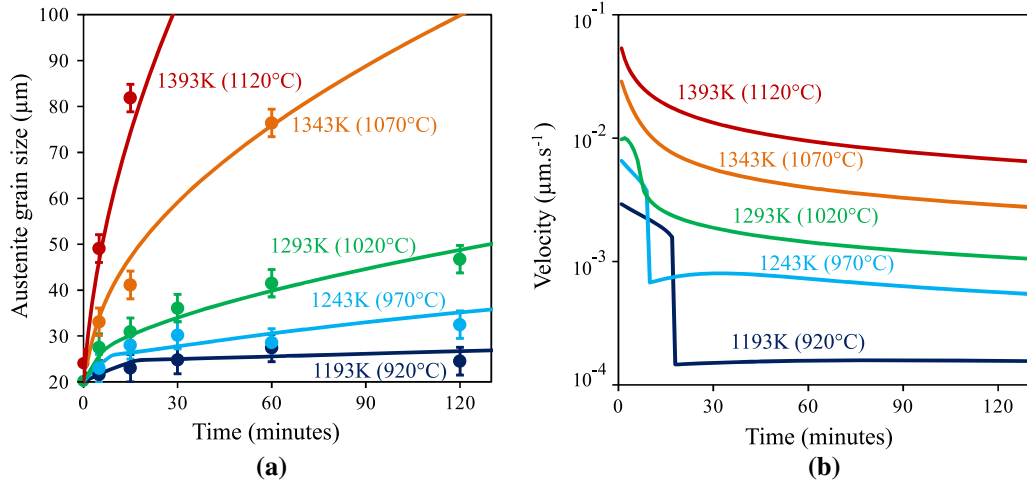
Fig. 9—(a) Comparison between austenite grain size as predicted from calculations (continuous lines) and experimental measurements (symbols), (b) evolution of predicted grain boundary velocity with time for all temperatures.

$$V_4 v_i^4 + V_3 v_i^3 + V_2 v_i^2 + V_1 v_i + V_0 = 0, \qquad [11]$$

where the expressions of V_0, V_1, V_2, V_3, and V_4 are as follows:

$$V_0 = k_d \gamma_g - P_z(i) D_{i-1}, \qquad [12]$$

$$V_1 = -2 P_z(i) dt - D_{i-1} (C_0 \alpha + M^{-1}), \qquad [13]$$

$$V_2 = (k_d \gamma_g - P_z(i) D_{i-1}) \beta^2 - 2 dt (C_0 \alpha + M^{-1}), \qquad [14]$$

$$V_3 = -\beta^2 (D_{i-1} M^{-1} + 2 dt P_z(i)), \qquad [15]$$

$$V_4 = -2 \beta^2 dt M^{-1}. \qquad [16]$$

To describe the evolution of precipitates during isothermal austenitization, results from MatCalc were fitted using an exponential law as a function of time in order to get a value of P_z for each iteration step i. The initial austenite grain size was set to $D_0 = 20$ μm based on experimental measurements (Figure 2), and the initial velocity was assumed to be 0.01 μm second^{-1}. The mobility M and the binding energy E_0 were taken as adjustable temperature-dependent parameters.

An algorithm was developed in order to resolve Eq. [11] for each time step t_i, $i \geq 1$, using the Newton's method. Since this equation has four possible solutions, the algorithm was forced to select the root closer to that of time step $(i - 1)$. A time step convergence analysis was conducted on the algorithm at three temperatures for $t = 1000$ seconds (16.6 minutes), using the parameters given in the next section. This duration was chosen because it corresponds to the beginning of the limited growth (Figure 2). The results converge (with respect to the time step) for a time step dt lower than 1 second (Figure 8(a)). Thus, a time step of 0.1 seconds was selected for the following calculations.

The mathematical validity of the algorithm was investigated. Assuming there are no pressures induced by the solute drag and the Zener pinning, the grain growth only depends on the driving pressure. In such case, Eq. [10] can be integrated as follows into an exact solution:

$$D = (D_0^2 + 4 M k_d \gamma_g t)^{1/2}, \qquad [17]$$

where Eq. [17] is the so-called parabolic growth law.[47]

For very small values of Zener and solute drag pressures, Eq. [17] can be considered as a reasonable approximation of the evolution of the grain size with time. Calculations were performed with the algorithm for such small pressures, *i.e.*, $E_0 = -0.1$ eV, $T = 1173$ K (900 °C), and $P_z = 10^{-3}$ MPa for different values of the mobility M. The resulting pressure induced by the solute drag is in the range of 10^{-4} MPa. Using these non-zero values of model parameters ensured that no simplification occurred in Eqs. [12] to [16], and that all mathematical terms were taken into account.

Comparison between the results from the parabolic growth law and predictions from the algorithm for $t = 120$ minutes are shown in Figure 8(b). Very good agreement is reached, with a relative difference below 5 pct, a large part of which is due to the retarding pressures. Indeed, the slight increase in the deviation observed with the increasing mobility is related to the decreasing driving pressure. As the driving pressure reaches a certain value, the retarding pressures can no longer be considered as negligible. It is worth mentioning that when retarding pressures are set to zero, the relative difference between Eq. [17] and the algorithm is less than 0.002 pct.

C. Model Predictions and Discussion

Comparison between model predictions using the values of M and E_0 is summarized in Table V, and experimental measurements is shown in Figure 9(a). Very good agreement is found. The model can thus be

used to examine the contribution of solute drag to the grain growth kinetics. The optimized values of model parameters are discussed at the end of this section.

Figure 10 shows the contributions of each different pressure on the total pressure exerted on the grain boundary at 1193 K (920 °C), 1243 K (970 °C), 1293 K (1020 °C), and 1343 K (1070 °C). As expected from the thermokinetic calculations, the Zener pressure only plays a small role in the grain growth kinetics, and is negligible at temperatures higher than 920 °C. Solute drag thus appears as the only mechanism responsible for limited growth observed at lower temperatures, *i.e.*, 1193 K (920 °C) and 1243 K (970 °C), and for slowed growth at 1293 K (1020 °C). Limited growth is due to the abrupt change in velocity observable in Figure 9(b) at 1193 K (920 °C) and 1243 K (970 °C), due to the transition from the high-velocity regime (low austenitization times) to the low-velocity regime of the solute drag equation. This transition results in an increase in pressure due to solute drag at 1193 K (920 °C) and 1243 K (970 °C), resulting in a drop in the total pressure which becomes very low. It occurs sooner at 1243 K (970 °C) since the diffusivity of molybdenum is higher at this temperature and therefore shifts the critical velocity toward higher values. Upon slowed growth, such

transition occurs as well but in a smoother manner, since the solute drag pressure (directly correlated to the binding energy) is smaller. At higher temperatures, the solute drag remains in the high-velocity regime and only has a small effect on grain boundary velocity.

It is noteworthy to mention that the predicted austenite grain size after 2 hours (120 minutes) at 1243 K (1070 °C) is 100 μm, in good agreement with the results reported in Table III (90 and 120 μm after 2 hours at 1323 K (1050 °C) and 1373 K (1100 °C), respectively).

1. Comments on optimized values of grain boundary mobility

The adjusted values of mobility are in the same order of magnitude as those reported for austenite grain growth accounting for solute drag and Zener pinning in an oxide dispersion-strengthened Fe-Cr alloy at 1623 K (1350 °C), namely 0.4 × 10^{-12} m^4 J^{-1} second^{-1}.[48]

The temperature dependency of the obtained values is well fitted by Eq. [3], where $M_0 = 4.67 \times 10^{-6}$ m^4 J^{-1} second^{-1} and $Q = 182$ kJ mol^{-1}, with a correlation coefficient of 0.99. As already stated, this activation energy is usually assumed to be within the range of 170 kJ mol^{-1}, *i.e.*, the activation energy for boundary
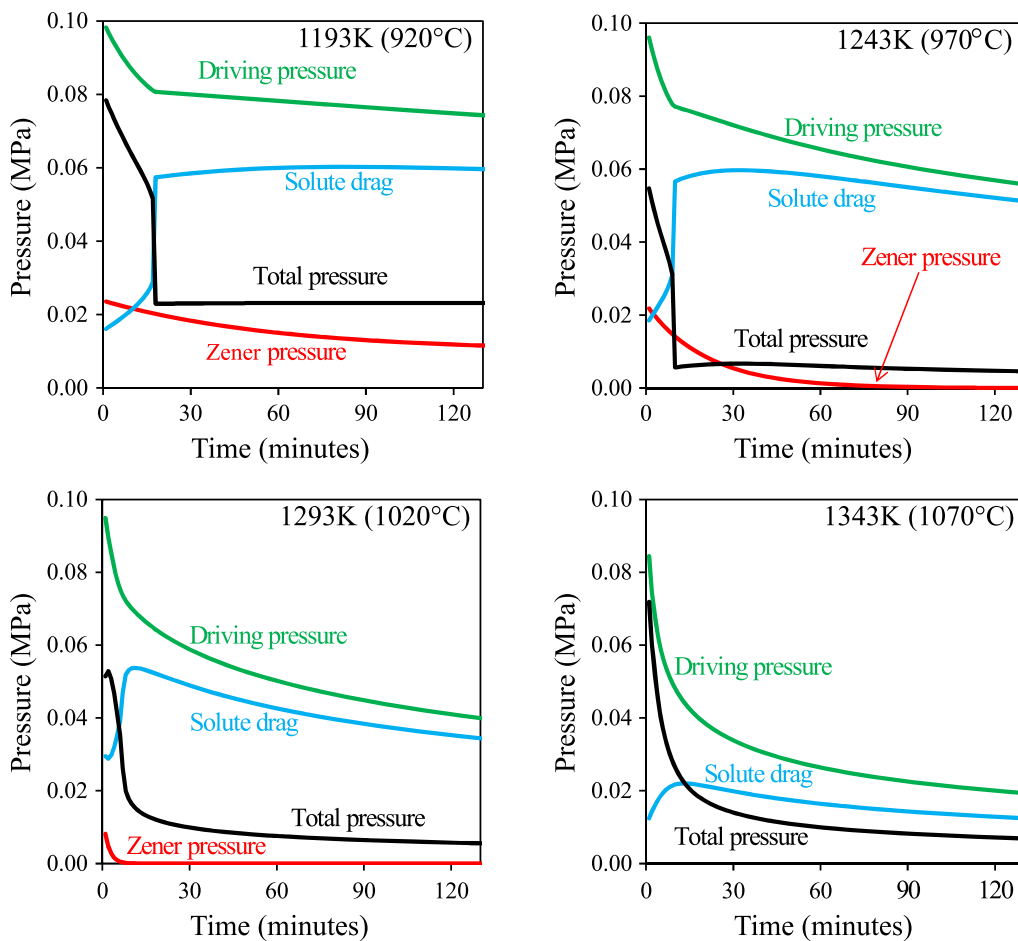

Fig. 10—Contributions from the different pressures exerted on the grain boundary at different temperatures.

diffusion of iron atoms in austenite, which is in rather good agreement with the value deduced from the present calculations.

At 1473 K (1200 °C), assuming that the solute drag is negligible and using a mobility as calculated with Eq. [3] and the obtained M_0 and Q parameters, the predicted austenite grain size after 2 hours of austenitization is 304 μm. This value is in very good agreement with the result reported in Reference 8 in Table III, namely 310 μm for the same austenitization heat treatment.

2. Comments on optimized values of binding energy

Optimized values of E_0 used in the calculations are in the upper limit of the expected range, which is consistent with the assumption that they represent effective binding energies accounting for the co-segregation of carbon and molybdenum. The best results were obtained with a binding energy varying with temperature (Table V), namely the binding energy decreasing for temperature equal to or higher than 1343 K (1070 °C). This can be explained using different assumptions. It was reported by Enomoto et al.[40] that the intensity of molybdenum segregation increases with the amount of carbon, and that carbon segregation at austenite grain boundaries increases due to the co-segregation of carbon and molybdenum. Moreover, this amount of segregated carbon and molybdenum decreases with temperature. Assuming that the effective binding energy of molybdenum to grain boundaries is a function of the amount of segregated carbon, the decrease in binding energy with increasing temperature appears credible. From the same study,[40] it was shown that the boundary energy decreases when the amount of carbon and molybdenum segregating at boundaries increases. As a result, the driving pressure would decrease too, as well as the retarding pressure needed to induce limited growth. Accounting for these considerations, the variation of binding energy with temperature might only be an artifact from calculations, necessary for counterbalancing the assumption about temperature-independent boundary energy. It should be pointed out that the interactions between neighboring grains are not taken into account in the present calculations. Such interactions lead to a decrease in the driving pressure, and thus, the binding energy inducing limited growth would be lower, as already discussed.

All these three considerations are likely to contribute to the rather high binding energies at lower temperatures and to their strong evolution with temperature. Nevertheless, whatever the values of binding energy, solute drag of molybdenum cannot be neglected in the limited or slowed down growth of austenite grain, and the current model gives qualitatively and quantitatively satisfactory results.

V. CONCLUSION

Experimental characterization and thermokinetic modeling of austenite gain growth in a vanadium-free 2.25Cr-1Mo steel led to the following conclusions:

- Limited growth is observed at 1193 K (920 °C) and 1243 K (970 °C); at 1293 K (1020 °C), the growth is only slowed down, and parabolic growth occurs at higher temperatures.
- Limited growth and slowed growth are due to the dragging of molybdenum atoms along the moving grain boundaries. Zener pinning by AlN precipitates only has a small or even negligible effect, depending on temperature.
- The relatively high binding energies between molybdenum atoms and austenite grain boundaries can be explained either by the co-segregation of molybdenum and carbon atoms or by an additional pressure exerted by the surrounding grains. In the latter case, the fact that the coefficient of variation for grain size distribution is independent of austenitization conditions may prove useful, as it gives the basis for a model where the growth of all grains would be represented, and thus where the competition between the driving pressures of neighboring grains would be taken into account.

REFERENCES

1. Y. Murakami, T. Nomura, and J. Watanabe: *Application of 2¼Cr-1Mo Steel for Thick-Wall Pressure Vessels*, ASTM, Denver, CO, 1982, pp. 383–417.
2. D.T. Blagoeva, L. Debarberis, M. Jong, and P. ten Pierick: *Int. J. Press. Vessels Pip.*, 2014, vol. 122, pp. 1–5.
3. R.L. Klueh: *Nucl. Eng. Des.*, 1982, vol. 72, pp. 329–44.
4. J. Orr, F.R. Beckitt, and G.D. Fawkes: *Ferritic Steels for Fast Reactor Steam Generators*, British Nuclear Energy Society, London, 1978, pp. 91–109.
5. T. Wada and G.T. Eldis: *Application of 2¼Cr-1Mo Steel for Thick-Wall Pressure Vessels*, ASTM, Denver, CO, 1982, pp. 343–61.
6. S. Suresh, G.F. Zamiski, and R.O. Ritchie: *Application of 2¼Cr-1Mo Steel for Thick-Wall Pressure Vessels*, ASTM, Denver, CO, 1982, pp. 49–67.
7. M. Pelletier: Study of Structural Transformations Occurring in Low Carbon Chromium-Molybdenum Ferritic Steels: Influence of Small Additions of Vanadium And Molybdenum. Ph.D. Dissertation, Paris-Sud University, Orsay, 1981.
8. S. Sato, S. Matsui, T. Enami, and T. Tobe: *Application of 2¼Cr-1Mo Steel for Thick-Wall Pressure Vessels*, ASTM, Denver, CO, 1982, pp. 363–83.
9. S. Dépinoy: Microstructural Evolution of a 2.25Cr-1Mo Steel During Austenitization and Temper: Austenite Grain Growth, Carbide Precipitation Sequence and Effects on Mechanical Properties. Ph.D. Dissertation, ENSMP, Paris, 2015.
10. H.J. Chang and J.J. Kai: *Scripta Metall. Mater.*, 1990, vol. 24, pp. 2101–06.
11. E. Bouyne: Propagation et arrêt de fissure de clivage dans l'acier 2¼Cr-1 Mo. Ph.D. Dissertation, ENSMP, Paris, 1999.
12. S.A. Khan and M.A. Islam: *J. Mater. Eng. Perform.*, 2007, vol. 16, pp. 80–85.
13. R.A. Swift: *Application of 2¼Cr-1Mo Steel for Thick-Wall Pressure Vessels*, ASTM, Denver, CO, 1982, pp. 166–89.

14. R.G. Ding, T.S. Rong, and J.F. Knott: *Mater. Sci. Technol.*, 2005, vol. 21, pp. 85–92.
15. T. Ishiguro, Y. Murakami, K. Ohnishi, and J. Watanabe: *Application of 21/4Cr-1Mo Steel for Thick-Wall Pressure Vessels*, ASTM, Denver, CO, 1982, pp. 129–47.
16. H.C.D. Nieuwland, S. Kawaguchi, H. Tsukada, K. Suzuki, I. Sato, J. Taira, and M. Kusuhashi: *Nucl. Eng. Des.*, 1985, vol. 84, pp. 123–46.
17. R.L. Bodnar, T. Ohhashi, and R.I. Jaffee: *Metall. Trans. A*, 1989, vol. 20, pp. 1445–60.
18. R.M. Miranda and M.A. Fortes: *Mater. Sci. Eng. A*, 1989, vol. 108, pp. 1–8.
19. S. Sista, Z. Yang, and T. Debroy: *Metall. Mater. Trans. B*, 2000, vol. 31, pp. 529–36.
20. F.J. Humphreys and M. Hatherly: *Recrystallization and Related Annealing Phenomena*, 2nd ed., Elsevier, Oxford, 2004, pp. 91–119.
21. H. Pous-Romero, I. Lonardelli, D. Cogswell, and H.K.D.H. Bhadeshia: *Mater. Sci. Eng. A*, 2013, vol. 567, pp. 72–79.
22. M. Maalekian, R. Radis, M. Militzer, A. Moreau, and W.J. Poole: *Acta Mater.*, 2012, vol. 60, pp. 1015–26.
23. M. Rath and E. Kozeschnik: *Mater. Sci. Forum*, 2013, vol. 753, pp. 357–60.
24. K. Banerjee, M. Militzer, M. Perez, and X. Wang: *Metall. Mater. Trans. A*, 2010, vol. 41, pp. 3161–72.
25. C.S. Smith: *Trans. Metall. Soc. AIME*, 1948, vol. 175, pp. 15–51.
26. P.A. Manohar, M. Ferry, and T. Chandra: *ISIJ Int.*, 1998, vol. 38, pp. 913–24.
27. S.F. Medina, M. Gómez, and P.P. Gómez: *J. Mater. Sci.*, 2010, vol. 45, pp. 5553–57.
28. M. Militzer, E.B. Hawbolt, T. Ray Meadowcroft, and A. Giumelli: *Metall. Mater. Trans. A*, 1996, vol. 27, pp. 3399–3409.
29. S. Maropoulos, S. Karagiannis, and N. Ridley: *J. Mater. Sci.*, 2007, vol. 42, pp. 1309–20.
30. J. Svoboda, F.D. Fischer, P. Fratzl, and E. Kozeschnik: *Mater. Sci. Eng. A*, 2004, vol. 385, pp. 166–74.
31. F.G. Wilson and T. Gladman: *Int. Mater. Rev.*, 1988, vol. 33, pp. 221–26.
32. S.P. Ringer, W.B. Li, and K.E. Easterling: *Acta Metall.*, 1989, vol. 37, pp. 831–41.
33. J.W. Cahn: *Acta Metall.*, 1962, vol. 10, pp. 789–98.
34. M. Bouet: The Effect of Molybdenum in Silicon-Manganese-Niobium TRIP Steels. Ph.D. Dissertation, McGill University, Montreal, 2000.
35. M. Enomoto, N. Maruyama, K.M. Wu, and T. Tarui: *Mater. Sci. Eng. A*, 2003, vol. 343, pp. 151–57.
36. N. Maruyama, G.D.W. Smith, and A. Cerezo: *Mater. Sci. Eng. A*, 2003, vol. 353, pp. 126–32.
37. H.A. Fletcher, A.J. Garratt-Reed, H.I. Aaronson, G.R. Purdy, W.T. Reynolds, Jr, and G.D.W. Smith: *Scripta Mater.*, 2001, vol. 45, pp. 561–67.
38. S.H. Song, R.G. Faulkner, and P.E.J. Flewitt: *Mater. Sci. Eng. A*, 2000, vol. 281, pp. 23–27.
39. J.L. Ham: *Trans. Am. Soc. Met.*, 1945, vol. 35, pp. 331–61.
40. M. Enomoto, C.L. White, and H.I. Aaronson: *Metall. Trans. A*, 1988, vol. 19, pp. 1807–18.
41. M. Guttmann, P. Dumoulin, and M. Wayman: *Metall. Trans. A*, 1982, vol. 13, pp. 1693–1711.
42. Z.-K. Liu: *Metall. Mater. Trans. A*, 1997, vol. 28, pp. 1625–31.
43. R.G. Faulkner: *Acta Metall.*, 1987, vol. 35, pp. 2905–14.
44. R.G. Faulkner, S.H. Song, and P.E.J. Flewitt: *Mater. Sci. Technol.*, 2013, vol. 12, pp. 904–10.
45. G.R. Purdy, W.T. Reynolds, Jr., and H.I. Aaronson: *Solid–Solid Phase Transformations*, The Japan Institute of Metals, Kyoto, 1999, pp. 1461–65.
46. M. Hoerner, M. Eberhart, and J. Speer: *Proc. 3rd World Congr. Integr. Comput. Mater. Eng.* (*ICME 2015*), Wiley, Hoboken, NJ, 2015, pp. 31–8.
47. J.E. Burke and D. Turnbull: *Prog. Met. Phys.*, 1952, vol. 3, pp. 220–92.
48. I. Toda-Caraballo, C. Capdevila, G. Pimentel, and C.G. De Andrés: *Comput. Mater. Sci.*, 2013, vol. 68, pp. 95–106.
49. L.M. Fu, H.R. Wang, W. Wang, and A.D. Shan: *Mater. Sci. Technol.*, 2011, vol. 27, pp. 996–1001.